ATLAS

P. Albicocco(Ass. Tecn.), M. Antonelli(Resp.), C. Arcangeletti (dott.),
M.M. Beretta, H. Bilokon, G. Ceccarelli(Tech.), S. Cerioni(Tech.),
V. Chiarella, M. Curatolo, R. Di Nardo,
E. Dane', G. Delle Monache, M. Dreucci,
B. Esposito, G. Ermini(Tech.), G. Fontana(Tech.),
C. Marini(Tech.), M. Gatta(Tech.),
P.F. Laurelli, S. Lauciani(Tech.),
G. Maccarrone, A. Martini, G. Mancini(Ass. Ric.),
D. Orecchini(Tech.), M. Paris (Tech.), G. Pileggi (Tech.),
B. Ponzio(Tech.), F. Putin(Tech.),
V. Russo(Tech.), A. Sansoni, F. Sborzacchi(Tech.),
M. Testa, S. Tomassini, P. T. Vassilieva(Tech.), E. Vilucchi.

In collaboration with:
Centro di Calcolo:
M. Pistoni, D. Spigone

May 9, 2019

1 Introduction

In the 2015-2018 data taking ATLAS collected proton-proton collisions at 13 TeV center of mass energy corresponding to an integrated luminosity of about 147 fb^{-1}.
Our group contributed significantly to the analysis $H \to ZZ \to 4\ell$ and Higgs Prospects as will be described in the following.
These contributions have been made possible also thanks to the reliability and the tools available on the LNF Tier2 approved by the INFN.
In parallel with the data taking activity, including shifts and maintenance, we are deeply involved in two upgrade Phase I activities: the Fast TracK (FTK) for the upgrade of the trigger system, and the new Small
Wheel for the upgrade of the muon system.
In addition we are strongly involved also to the upgrade Phase II activity concerning the Inner Tracker (ITk).

2 Tier-2

During the year 2018 the Frascati Tier2 successfully and continuously performed all the typical activities of an ATLAS Tier-2: Monte Carlo production and users and physics groups analysis; then the PADME experiment started its activity in the Tier2 farm storing raw, MC and reconstructed data in the storage system and running MC, reprocessing and analysis jobs in the Tier2 cluster, with pledged resources. During the year, the Tier2 farm has reached 24 kHEPSPEC of computing power and about 2 PB of disk space, running also the computing activities of the following Virtual Organizations (VO): LHCb, Belle, CTA and KM3Net.
Among the activities that involved the Tier-2 staff we mention the role of VO manager for ATLAS VO (recognized as in kind contribution of the Italian group) and software VO manager for KM3Net VO.
For what concern the Grid middleware, during 2018 the Tier-2 staff continued to test and develop the cache systems, with the DPM storage system, in collaboration with the Italian ATLAS Tier-2 federation staff and as part of the IDDLS (Italian Distributed Data Lake for Science) project. Moreover the LNF Tier2 was involved in the presentation of the computing PON Ibisco to host the computational resources of the CTA INAF experiment.

3 FTK

The trigger is a fundamental part of any experiment at hadron colliders. It is needed to select on-line the interesting low cross-section physics from the huge QCD background. Experience at high luminosity hadron collider experiments shows that controlling trigger rates at high instantaneous luminosity can be extremely challenging. As the luminosity increases, physics goals change in response to new discoveries, and detector aging. It is thus essential that the

trigger system be flexible and robust, and redundant and significant operating margin. Providing high quality track reconstruction over the full ATLAS Inner Detector by the start of processing in the level-2 computer farm can be an important element in achieving these goals. With the goal to improve and make more robust the ATLAS trigger, during summer 2007 the group joined the Fast-Track (FTK) proposal for A hardware track finder for the ATLAS trigger. This is a proposal to build a hardware track finder as an upgrade to the ATLAS trigger. It will provide global reconstruction of tracks above 1 GeV/c in the silicon detectors, with high quality helix parameters, by the beginning of level-2 trigger processing. FTK can be particularly important for the selection of 3rd-generation fermions (b and τ). These have enormous background from QCD jets, which can be quickly rejected in level-2 if reconstructed tracks are available early. This RD proposal was completed with the submission of the FTK Technical Proposal that was finally approved by the ATLAS collaboration meeting in June 2011.
Under the FTK context we contributed in the development and test of the Associative Memory (AM) chips for track detection and the FTK Input Mezzanines (IMs) boards for hit information clustering.

3.1 FTK Input Mezzanines

The FTK IMs boards receive data to be processed from the detectors Read Out Drivers (RODs) over 380 S-Link for a total input rate of $760 Gbps$. Each board receives data over four optical links at $2 Gbps$, performs an early reduction of the data to optimize the subsequent FTK processing and transmits forward the clustered data by a $200 MHz\ DDR$ signalling over 16 LVDS pairs.
Due to the high occupancy of the IBL ATLAS pixel layer, the previous version of the FTK IM board based on Xilinx Spartan6 FPGA could not process all the data coming from the detector. We have developed this board together with FTK Japanese group of Waseda University. As responsible of this board the FTK collaboration ask us to develop a new version of the FTK IM based on a Xilinx Artix7 FPGA. This is a more recent and powerful FPGA.
The new board have been designed in 2014, Figure 1.
During 2017 the firmware of the Artix-7 IM has been constantly kept updated. The main activities has been the maintenance of the mezzanine with problems.

3.2 FTK AMCHIP06 test

In 2017 was started the AMchip06 mass production test at Microtest. LNF is involved in the test of this chip with these items:

- design a new test board without low drop voltage regulator;
- organizing and following the mass production test with external company.

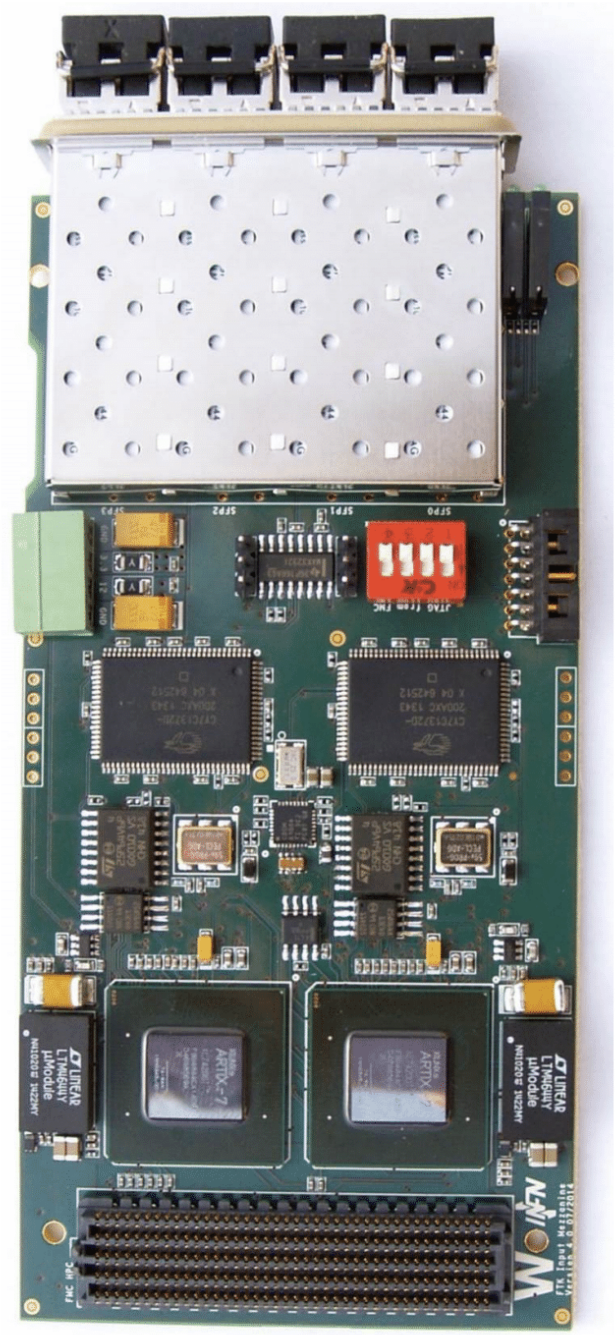

Figure 1: Artix7-IM

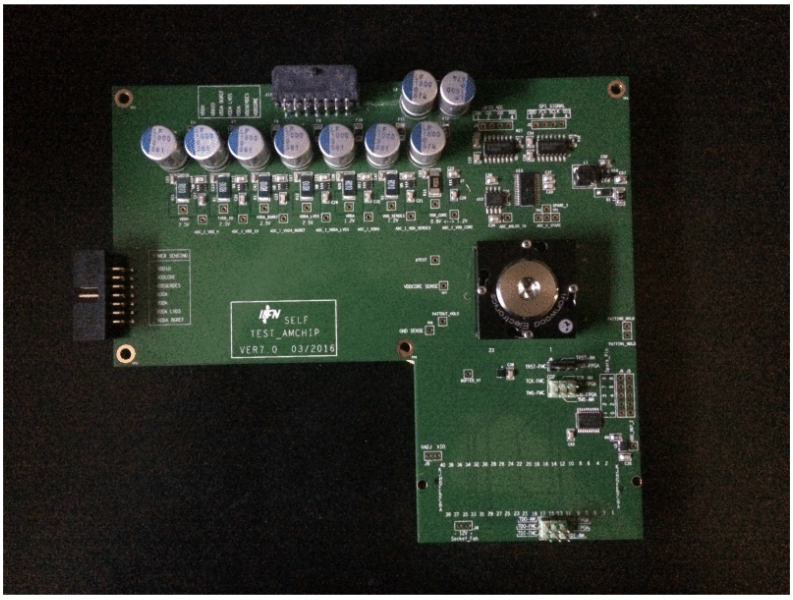

Figure 2: New test board for the AMchip06

In the following paragraph the listed items will be described.
The test board for the Amchip06 was re-designed to be compatible with new socket with mechanical spring contacts. The previous socket, with elastomer contacts, has shown reliability problems after few thousands of tested components (usually we have problems after 2000 components tested). We have to test about 20000 chips, so we have decided to change the socket with a more reliable and expensive one, in order to guarantee the correct level of reliability in the test results.
The specification used to design the board was the following:

- FMC HPC connector
- On Board 100MHz clock
- FMC alternative clock distribution
- 12 differencial high speed (2.5 GHz) lines
- On board power supply current and voltage monitor

The board designed with all features highlighted are shown in the picture 2
We are constantly in contact with the company in charge of the tests to give help in maintenance of the test system.

4 New Small Wheel upgrade project: Micromegas [1] [2]

MicroMegas (MM) chambers is an abbreviation for MICRO MEsh GASeous Structure and it is an innovative design concept for Micro-Pattern Gaseous Detectors first introduced by Charpak and Giomataris during the 1990s. These chambers have been chosen as new precision tracking detectors for the upgrade of the forward muon spectrometer of the ATLAS experiment at the Large Hadron Collider (LHC) during the second long shut-down of the LHC [3]. MicroMegas are gas detectors in which a 5 mm gap between two parallel electrodes is filled with a $93:7$ $Ar:CO_2$ gas mixture and a thin metallic micromesh is placed between the two electrodes, held by pillars with a pitch of few millimeters and a height of about 128 μm. The drift electrode, with a -300 V voltage applied, and the mesh, which is grounded, define the drift region, where the ionisation takes place and the low electric field ($\sim$600V/cm) leads the produced electrons towards the mesh. Following the field lines the electrons enter the very thin amplification region between the mesh and the readout electrode, which is segmented into strips with a pitch of about 400 μm, where a 500 - 600 V voltage is applied. Due to the very high electric field (40 - 50 kV/cm) the electrons produce avalanches with a gain of the order of 104. The thin amplification gap allows a fast ions evacuation, which occurs in about 100 ns, and allows MM to operate in highly irradiated environments. MM chambers are designed to provide a space resolution below 100 μm and a tracking efficiency better than 95% per single plane. The produced signal is then read by the readout strips capacitively coupled to the resistive ones in order to reduce the performance degradation due to discharges in the detector. INFN is deeply involved in the Micromegas Chambers construction and testing of the new chambers at the LNF Cosmic Ray Stand. At the LNF an assembly procedure of the chambers to guarantee the alignment of the readout strips has been developed, together with a validation procedure to test the functioning of the detectors.

4.1 Production Scheme

The NSW structure consist of 8 large sectors and 8 small sectors, with 2 modules per sector and 4 MM quadruplets. MM chambers are therefore produced in 4 different shapes: LM1, LM2, SM1, SM2. The production is distributed over different institutes and industries: Germany(SM2), France(LM1), Russia-Greece-CERN (LM2) and Italy is responsible for the SM1 construction. The INFN has been committed to built 32 quadruplets. The INFN Italian production is summarized as shown in Figure 3.

4.2 Assembly and Validation Procedure

A MicroMegas module is made of four gas gap (*Quadruplet*) and it consists of 5 panels: two outer Drift panels, one central Drift Panel and two Readout

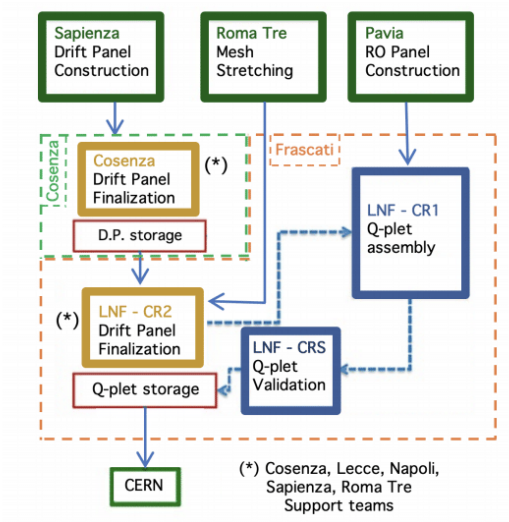

Figure 3: INFN production scheme of SM1.

panels, the *Eta* (with vertical strip to measure the η coordinate) and the *Stereo* (with strip tilted at $\pm 1.5°$ to measure the ϕ coordinate). A *cleaning procedure* of the panels, using micro-polishing detergent and deionised water, has been developed during this year to remove the most of the contaminants that remain on the panels surface during the production phases and lead to HV issues. The assembly procedure of a module takes place in the clean room, with the use of purpose-built tools to close the module in a vertical way, to reduce the dust deposits and guarantee a good alignment between the two readout panels using load cells. The assembly starts from the closure of the first gap with an outer Drift panel and the Stereo Readout panel and its HV test in air and in $Ar : CO_2$. Then the procedure continues with the assembly of the central Drift, the Eta Readout and the last outer Drift panel. The high voltage test is done on each gap.
At the end of the assembly, when the quadruplet is closed, a series of validation test is done:

- *Planarity and Thickness.* The Quadruplet is positioned on several supports, which represents the reference plane (z=0) for planarity and thickness measurements. All measurements has been made with a Laser Tracker and doing a fit of the cloud points for each side of the quadruplet.

- *Gas Leak Test.* The module is pressurized at $\sim$3 mbar and the pressure drop is monitored to estimate the leak of the chamber.

- *Strip Alignment.* The alignment between the readout-strips of the four

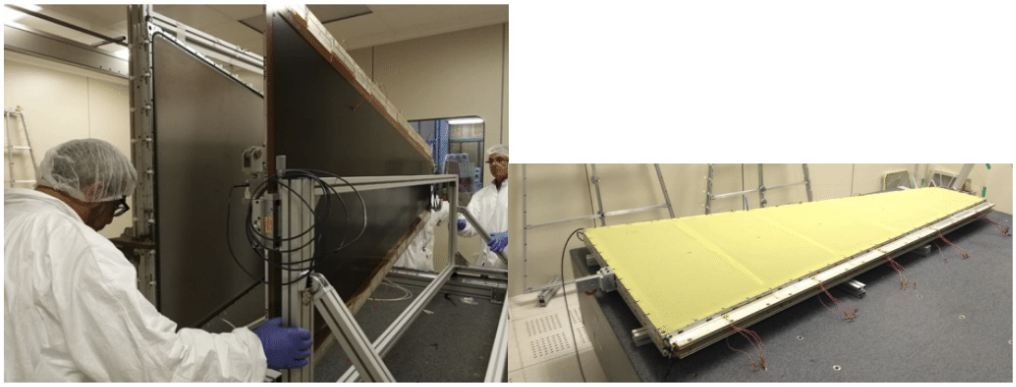

Figure 4: *On the left*: closure of the first gap with the panel positioned on the vertical tools. *On the right*: the assembled quadruplet positioned on the supports ready for the validation measurements in clean room.

layers of the module is measured using the *Double-RasFork*, a tool that reads the coded masks on the side of the PCBs with a contact-CCD installed on it.

- *High Voltage Test.* A slow high voltage *conditioning* procedure is performed for each module. It start applying a voltage of 400 V in the amplification region, and it slowly increases until it reaches the nominal working point for the SM1 module of 570 V.

4.3 Cosmic Ray Stand Test

The modules need to be validated at the Cosmic Ray Stand to estimate the efficiency and the gain uniformity of each chambers.
The experimental setup (Figure 5) currently consists of two scintillators for the trigger coincidence separated by 35 cm of iron, achieving a trigger rate of 50 Hz. The Signals from the read-out strips are read using APV25 front-end readout electronics which provides the collected charge as a function of the time in 25 ns bins. By fitting the risetime of the distribution with an inverse Fermi-Dirac function, the time of the arrival of the signal, defined as the inflection point of the function, and the charge induced on the strip, defined as the maximum of the distribution subtracted by the baseline level, can be measured. For each strip i the time t_i and the charge q_i are therefore measured and clusters are reconstructed as groups of neighboring strips according to dedicated clustering algorithms.
Up to now 14 modules has been produced and fully assembled by the INFN group and we have tested and validated 8 chambers. Two modules has been installed on the first Double-Wedge of the New Small Wheel.

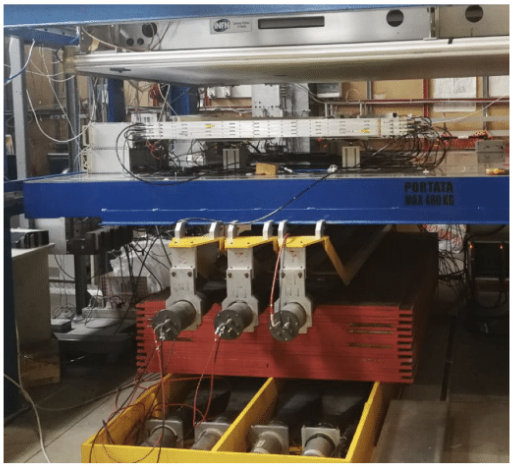

Figure 5: Experimental setup at the ATLAS LNF Cosmic Ray Stand.

4.4 Results of a SM1 module produced by INFN

In this section the results of one of the produced and validated modules are shown. In Figure 6 the planarity plot of the point cloud of one side is shown, in Figure 7 the pressure drop plot is shown, in Figure 8 the scheme of the displacement of the coded masks on the PCBs side, and then of the readout strips, between the Eta and the Stereo readout panel is shown and finally in Figure 9 the plot of the efficiency per Layer are represented.

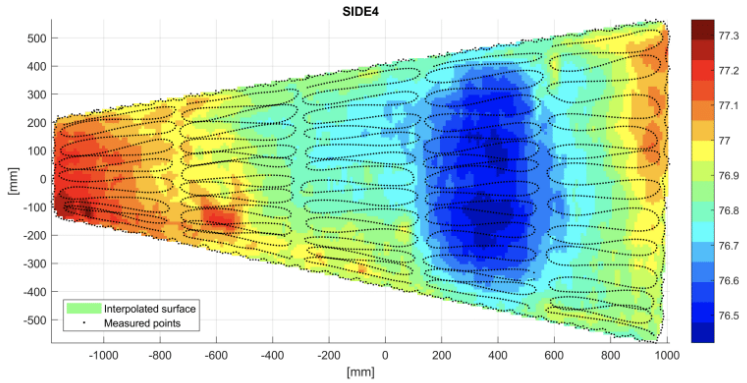

Figure 6: Point cloud obtained with the Laser Tracker on one side of the module for the planarity and thickness measurements.

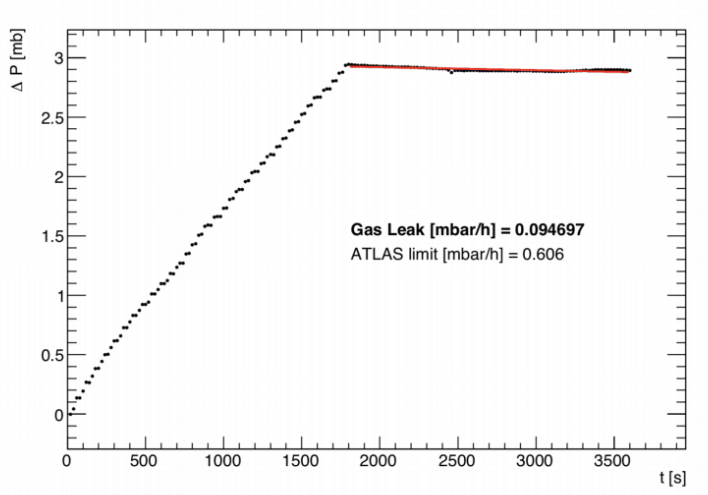

Figure 7: Pressure drop plot to measure the gas tightness of the chamber.

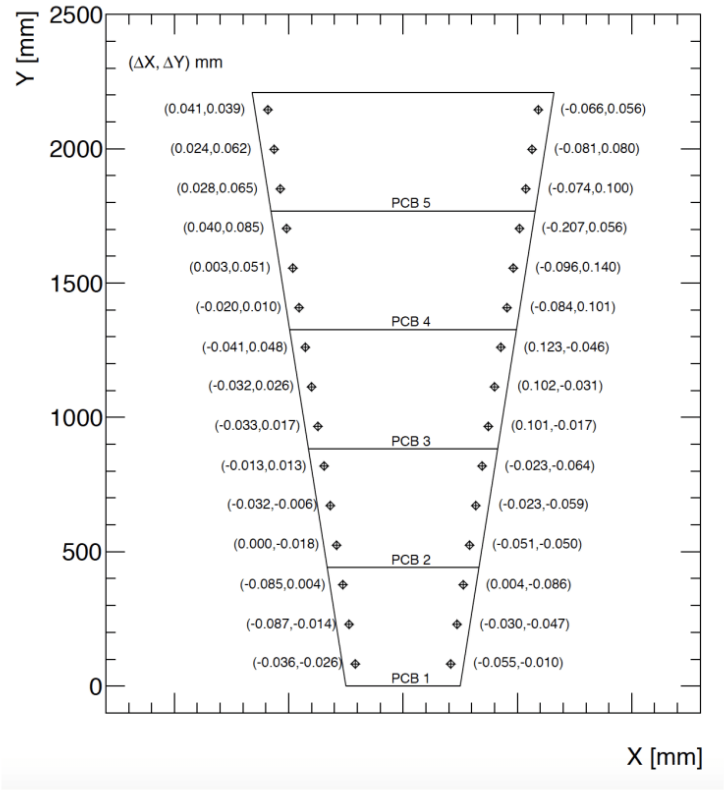

Figure 8: Scheme of the ΔX and ΔY displacement of the readout strips between the Eta and the Stereo readout panel.

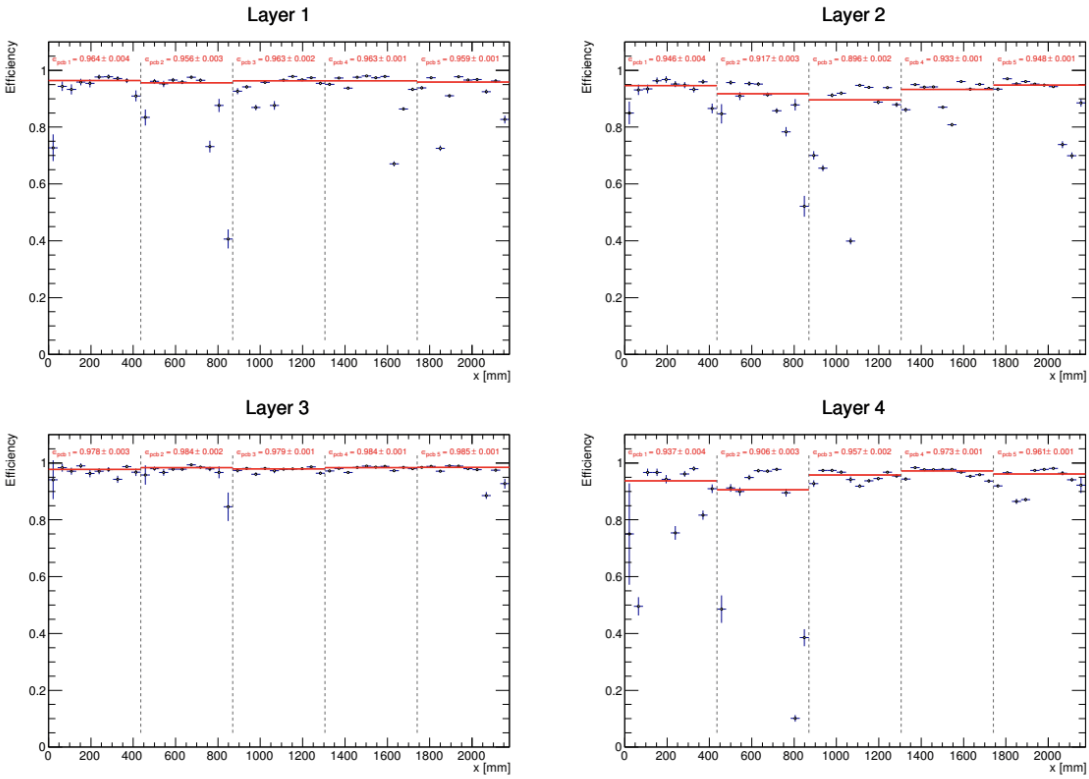

Figure 9: Efficiency plot per Layer.

Responsibilities

- G.Mancini, supervisor of Gianluca Zunica's master thesis *Rivelatori Micromegas per lo spettrometro di muoni in avanti dell esperimento ATLAS a LHC*
- G.Mancini, review of paper JINST Paper Construction and Test of a small-pad resistive Micromegas prototype (JINST_030P_0818)
- G.Mancini, Co discussion leader at the XIX Frascati Spring School "Bruno Touschek" in Nuclear, Subnuclear and Astroparticle Physics, 7 - 11 May 2018
- G.Mancini, corresponding author of a Nuclear Instrumentation Module (NIM) article concerning the construction techniques and the performance studies on the Micromegas chambers built for the upgrade of the innermost station of the ATLAS Muon spectrometer

Public presentations and posters:

- G.Mancini, *Construction and test of SM1 Micromegas chambers for the upgrade of the ATLAS Muon spectrometer*, Talk presented at XIX Frascati Spring School "Bruno Touschek" in Nuclear, Subnuclear and Astroparticle Physics, 7 - 11 May 2018
- G.Mancini, *Construction and test of SM1 Micromegas chambers for the upgrade of the forward muon spectrometer of the ATLAS experiment*, Poster presented at PM2018 (Pisa Meeting on Advanced Detectors, La Biodola), 27 May - 2 June 2018
- G.Mancini, *SM1 Report on HV Stability*, Talk presented at the Micromegas Technical Review (https://indico.cern.ch/event/746977/)
- G.Mancini, *SM1 Status Report on assembly status, cleaning procedure, HV studies*, Talk presented at the ALAS Muon Week, 18 June 2018
- G.Mancini, *Frascati Proposal for the gas-gap frame machining*, Talk presented at the Micromegas Mini-Workshop day 1, 16 April 2018
- G.Mancini, *SM1 report on Cleaning Status, Infrastructures Readiness and HV Results*, Talk presented at the Micromegas Mini-Workshop day 2, 17 April 2018
- G.Mancini, *Costruzione e test delle camere Micromegas SM1 per l'upgrade dello spettrometro a muoni dell'esperimento ATLAS*, Talk presented at IFAE 2018 (Incontri di Fisica delle Alte Energie, Milano), 4-6 April 2018
- G.Mancini, *Measurement of the Higgs boson properties at the ATLAS experiment*, Talk presented at SILAFAE (Latin American Symposium on High Energy Physics, Lima), 26-30 November 2018

- C. Arcangeletti, *Assemblaggio e validazione delle camere Micromegas per l'esperimento ATLAS*, Talk presented at 104° Congresso Nazionale della Societ Italiana di Fisica, Cosenza and Rende (Italy), 17-21 September 2018

5 Study on the properties of the Higgs boson in the $H \to ZZ^* \to 4l$ decay channel

The ATLAS detector collected proton-proton collisions at 13 TeV center of mass energy between 2015 and 2017 data taking at LHC, corresponding to an integrated luminosity of $79.8 \pm 1.6 fb^{-1}$.
Back on 4 July, 2012, the LHC experiments reported the evidence of an Higgs boson-like particle with a mass of about of 125 GeV and great interest has been posed on the measurements of its properties to assure whether it is the Standard Model (SM) Higgs boson or not. In this context, during the Run2 at LHC, with an increased center of mass energy of the collisions, the measurement of the Higgs properties remains one of the main goals of the physics program since hints of New Physics (NP) effects can be hidden in the Higgs sector. Deviations from the SM expectations could indicate exotic properties of the Higgs or presence of exotic particles in association with Higgs. Studies performed during Run1 showed that deviations from the SM expectations in the Higgs sector are small: the Higgs quantum numbers are measured to be $J^P = 0^+$ (alternative hypotheses are excluded with a 99.9% C.L.), its signal strength ($\mu = Ev_{obs}/Ev_{SM}$) and coupling measurements to vector bosons and fermions are found to be consistent with the SM with an accuracy of the order of 10%.
In the $H \to ZZ^* \to 4\ell$ final state, the first measurement in Run2 have been focusing on the Higgs boson coupling to SM particles. The measurement has been performed dividing the events in categories built depending on the characteristic of the event, aiming for discrimination between production modes. The measurement of the cross section per production mode has been performed, together with the measurement of the Higgs boson couplings to bosons and fermions.
In the SM, the Higgs boson is a $\mathcal{CP}$-even scalar particle ($J^{\mathcal{CP}} = 0^{++}$) and theories of physics BSM often require an extended Higgs sector featuring several neutral Higgs bosons. Such cases may include $\mathcal{CP}$-mixing in the Higgs boson interactions, which could result in observable differences in the kinematics of final-state particles produced in their decays, or from Higgs boson production, such as in VBF interactions.
The possible presence of BSM terms in the Lagrangian describing the spin-0 resonance is investigated describing the HVV vertex interaction in terms of an effective BSM $\mathcal{CP}$-odd and $\mathcal{CP}$-even operators and deriving limits on the corresponding BSM tensor couplings are derived. Our group contributed significantly to this studies ([4]) with fundamental contributions to the

analysis and to the measurement of the Higgs boson properties in the $H \to ZZ^* \to 4\ell$ decay channel.

5.1 Cross section per production mode measurements

In order to measure the cross sections per production mode, categories enriched in each Higgs production mechanism have been defined (Figure 10). The Higgs boson production cross section times the branching ratio of the decay into Z boson pairs, $\sigma \times BR(H \to ZZ^*)$, is measured in several dedicated mutually exclusive regions of the phase space based on the production process which are called production bins. The bins are chosen in such a way that the measurement precision is maximized and at the same time possible BSM contributions can be isolated. All production bins are defined for Higgs bosons with rapidity $|y_H| < 2.5$ and no requirements placed on the particle-level leptons. Two sets of production bins are considered since a more inclusive phase-space region usually reduces the statistical uncertainty of the measurement but at the cost of a larger theoretical uncertainty.
For the first set (Stage 0), production bins are simply defined according to the Higgs boson production vertex: gluon-gluon fusion (ggF), vector boson fusion (VBF) and associated production with top quark pairs (ttH) or vector bosons (VH), where V is a W or a Z boson. The bbH Higgs boson production bin is not included because there is insufficient sensitivity to measure this process with the current integrated luminosity. This production mode has an acceptance similar to gluon-gluon fusion, and their contributions are therefore considered together in the analysis. The sum of their contributions is referred to in the following as gluon-gluon fusion.
For the second set (reduced Stage 1), a more exclusive set of production bins is defined. There are eleven reconstructed event categories defined for the cross-section measurement, one of which is additionally split into two separate ones for the tensor structure studies to improve their sensitivity. For the cross section measurement, there are also additional discriminating observables introduced in reconstructed event categories with a sufficiently high number of events. These observables are defined using dedicated boosted decision trees (BDTs). The expected number of SM Higgs boson events with a mass $m_H = 125.09$ GeV in the mass range $118 \leq m_{4l} \leq 129$ GeV for an integrated luminosity of $79.8 fb^{-1}$ and $\sqrt{s} = 13$ TeV in each reconstructed event category is shown separately for each Stage-0 production bin in Figure 11. The ggF and bbH contributions are shown separately but both contribute to the same (ggF) production bin. Statistical and systematic uncertainties are added in quadrature. Figure 12 shows the fraction of signal events in each category per production modes, showing the extreme purity of some categories. The ggF and bbH contributions are shown separately but both contribute to the same (ggF) production bin. The relation between N_k^{obs}, the observed number of

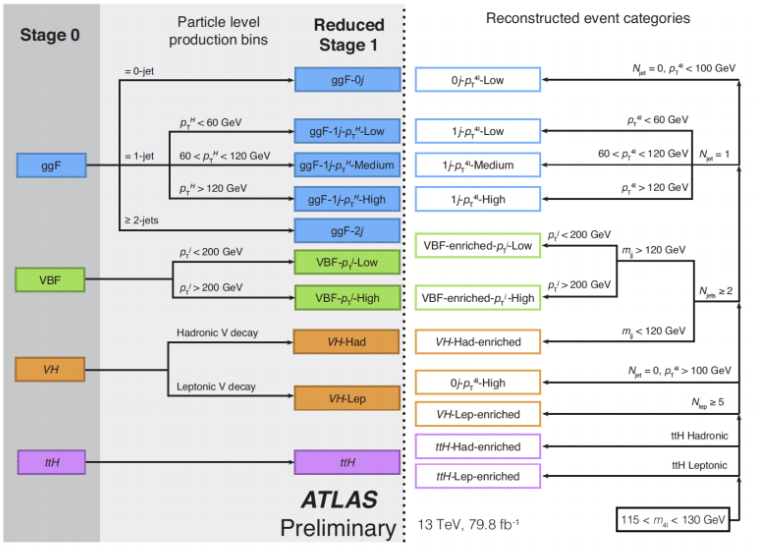

Figure 10: Event categorization scheme.

Reconstructed event category	SM Higgs boson production mode ggF	VBF	WH	ZH	$t\bar{t}H$	$b\bar{b}H$	tH
$0j$-p_T^{4l}-Low	54 ± 5	0.64 ± 0.12	0.213 ± 0.032	0.199 ± 0.030	-	0.56 ± 0.28	-
$1j$-p_T^{4l}-Low	16.1 ± 2.2	1.05 ± 0.06	0.291 ± 0.035	0.173 ± 0.021	0.0017 ± 0.0010	0.23 ± 0.12	0.00140 ± 0.00030
$1j$-p_T^{4l}-Med	9.6 ± 1.5	1.38 ± 0.15	0.292 ± 0.033	0.194 ± 0.022	0.0018 ± 0.0011	0.049 ± 0.025	0.0021 ± 0.0004
$1j$-p_T^{4l}-High	2.4 ± 0.5	0.60 ± 0.07	0.115 ± 0.014	0.106 ± 0.013	0.0018 ± 0.0006	0.009 ± 0.004	0.0017 ± 0.0004
VBF-enriched-p_T^j-Low	7.8 ± 1.6	4.1 ± 0.4	0.35 ± 0.05	0.29 ± 0.04	0.124 ± 0.013	0.10 ± 0.05	0.055 ± 0.007
VBF-enriched-p_T^j-High	5.5 ± 1.1	0.43 ± 0.04	0.68 ± 0.07	0.52 ± 0.05	0.051 ± 0.008	0.053 ± 0.027	0.0169 ± 0.0022
VH-Had-enriched	0.70 ± 0.20	0.38 ± 0.04	0.062 ± 0.010	0.050 ± 0.008	0.038 ± 0.005	0.0014 ± 0.0007	0.0119 ± 0.0013
VH-Lep-enriched	0.030 ± 0.004	0.0084 ± 0.0004	0.44 ± 0.04	0.116 ± 0.011	0.083 ± 0.011	0.0028 ± 0.0014	0.0172 ± 0.0018
$0j$-p_T^{4l}-High	0.059 ± 0.022	0.0096 ± 0.0017	0.030 ± 0.004	0.085 ± 0.010	-	-	-
$t\bar{t}H$-Had-enriched	0.09 ± 0.09	0.020 ± 0.004	0.0130 ± 0.0027	0.028 ± 0.006	0.38 ± 0.04	0.012 ± 0.006	0.054 ± 0.006
$t\bar{t}H$-Lep-enriched	-	-	0.0026 ± 0.0006	0.0018 ± 0.0004	0.212 ± 0.025	-	0.0204 ± 0.0022
Total	97 ± 8	8.6 ± 0.4	2.49 ± 0.25	1.76 ± 0.17	0.90 ± 0.09	1.0 ± 0.5	0.181 ± 0.020

Figure 11: The expected number of SM Higgs boson events with a mass $m_H = 125.09$ GeV in the mass range $118 \leq m_{4l} \leq 129$ GeV for an integrated luminosity of $79.8 fb^{-1}$ and $\sqrt{s} = 13$ TeV in each reconstructed event category.

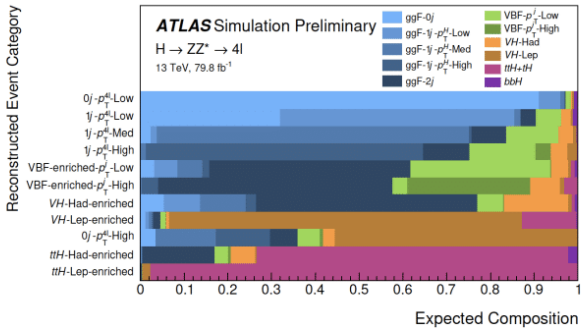

Figure 12: Signal composition in terms of the reduced Stage-1 production bins in each reconstructed event category.

events in each analysis categories (denoted as k), and the cross section in each truth bin σ_i^j (i denotes different production mechanisms and j denotes the index of a phase space or truth bin in the simplified template cross section binning scheme), can be expressed as follows:

$$\mathcal{N}_k^{\text{obs}} = \mathcal{L}_{\text{int}} \times \mathcal{BR}_{H\to ZZ^*\to 4\ell} \times \left(\sum_{i=1}^{\mathcal{N}^{prod}} \sum_{j=1}^{\mathcal{N}_{bin}^i} \mathcal{A}_{kj}^i \sigma_i^j \right) \tag{1}$$

where $\mathcal{L}_{\text{int}}$ is the integrated luminosity, $\mathcal{N}^{prod}$ is the number of Higgs production mechanisms, $\mathcal{N}_{bin}^i$ is the number of truth bins per Higgs production mechanism i, $\mathcal{A}_{kj}^i$ takes into account for detector response (trigger, reconstruction and identification efficiencies) for detecting the final state and the kinematic and geometric acceptance for the truth bin j of Higgs production mechanism i in the analysis category k.
Assuming that the relative signal fractions in each production bin are given by the predictions for the SM Higgs boson, the inclusive production cross section of

$$\sigma \times BR(H \to ZZ^*) = 1.57 \pm 0.15(stat.) \pm 0.08(exp.) \pm 0.04(th.) pb = 1.57 \pm 0.18 pb \tag{2}$$

is measured in the rapidity range $|y_H| < 2.5$, compared to the SM prediction of

$$(\sigma \times BR(H \to ZZ^*))_{SM} = 1.33 \pm 0.09 pb \tag{3}$$

The data are also interpreted in terms of the global signal strength, yielding

$$\mu = 1.19 \pm 0.12(stat.) \pm 0.06(exp.)^{+0.08}_{-0.07}(th.) = 1.19^{+0.16}_{-0.15} \tag{4}$$

Results are extracted from fits to the data using the profile likelihood ratio. Figures 13 show the results in terms of cross sections per production mode respectively for the Stage0 and Stage1 cases.

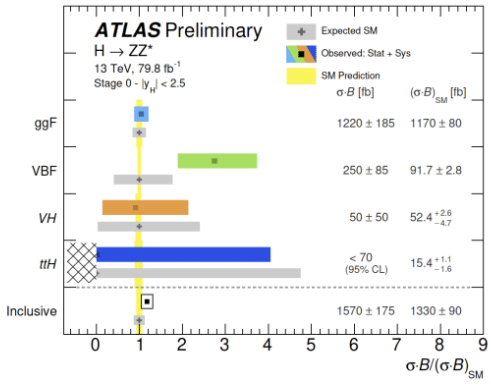

(a)

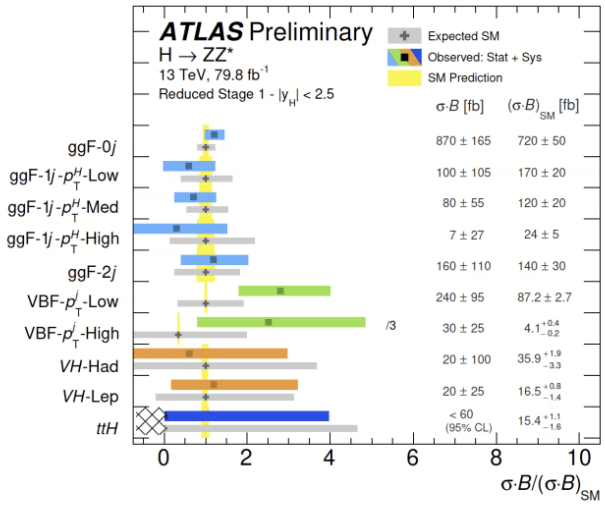

(b)

Figure 13: . The observed and expected SM values of the cross-section ratios $\sigma \times BR$ normalized by the SM expectation for the inclusive production and in the (a) Stage0 and (b) reduced Stage-1 production bins for an integrated luminosity of 79.8 fb^{-1} at $\sqrt{13}$ TeV. Different colors for the observed results indicate different Higgs boson production modes. The hatched area indicates that the ttH parameters of interest are constrained to positive values. For visualization purposes, the VBF-p_{Tj}-High value is divided by a factor of three when shown normalized to $\sigma \times BR_{SM}$. The yellow vertical band represents the theory uncertainty in the signal prediction, while the horizontal grey bands represent the expected measurement uncertainty.

Figure 14 shows the likelihood contours in the
$(\sigma_{ggF} \cdot BR(H \to ZZ^*), \sigma_{VBF} \cdot BR(H \to ZZ^*))$ and
$(\sigma_{VBF} \cdot BR(H \to ZZ^*), \sigma_{VH} \cdot BR(H \to ZZ^*))$ plane. The other cross section parameters are left free in the fit, i.e. they are not treated as parameters of interest. The compatibility with respect to the Standard Model expectation is at the level of 2.1 and 1.9 standard deviations in the
$(\sigma_{ggF} \cdot BR(H \to ZZ^*), \sigma_{VBF} \cdot BR(H \to ZZ^*))$ and
$(\sigma_{VBF} \cdot BR(H \to ZZ^*), \sigma_{VH} \cdot BR(H \to ZZ^*))$ plane respectively.

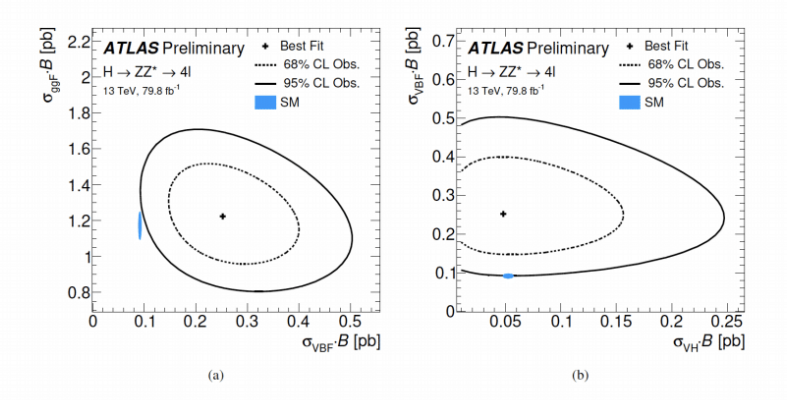

Figure 14: Likelihood contours at 68% CL (dashed line) and 95% CL (solid line) in the (a) $(\sigma_{ggF} \cdot BR(H \to ZZ^*), \sigma_{VBF} \cdot BR(H \to ZZ^*))$ and (b) $(\sigma_{VBF} \cdot BR(H \to ZZ^*), \sigma_{VH} \cdot BR(H \to ZZ^*))$ plane. The SM predictions is shown together with its uncertainty (filled blue ellipse).

Responsabilities:

- G.Mancini Editor of the supporting documentation for the $H \to ZZ^* \to 4l$ coupling measurements

6 Projections for measurements of Higgs boson properties at the HL-LHC

In 2018, in view of the update of the European strategy, the LHC experiments have provided a large number projections of the measurements expected at HL-LHC. One of the most important part of the physics program at HL-LHC is the precise measurement of Higgs boson properties [7]. The results on the Higgs couplings using data collected in 2015, 2016 and 2017, 36 fb^{-1} or 80 fb^{-1}, have been extrapolated to $3000 fb^{-1}$, which is the integrated luminosity

expected to be collected in ten years of HL-LHC operations. The extrapolations account also for the increase in total cross sections from 13TeV in Run2 data to 14 TeV at HL-LHC.
The object reconstruction efficiencies, resolutions and fake rates are assumed to be similar in the Run 2 and HL-LHC environments. This is based on the assumption that the improved performance of the ATLAS detector at HL-LHC will compensate for the degradation induced by higher pile up. Systematic uncertainties are separated into components for experimental uncertainties and theory uncertainties on signal and background processes. In the baseline scenario for these projections, their values are reduced compared to those currently used in Run 2, reflecting the situation that is expected to be reached at the end of the HL-LHC programme. By default, most of theory uncertainties for signal and background are halved. The uncertainty on the integrated luminosity is set to 1%. The uncertainties due to the limited size of simulation samples are assumed to be negligible. In the relevant analyses, the uncertainty on the modeling of the continuum background using a functional form description is also assumed to become negligible. In Fig. 15, left, the expected precision for the cross section times branching ratios are shown. On the right, the expected precision for the coupling of the Higgs Bosons per particle type is observed. The rare channel $H \to \mu\mu$ decay, not yet observed, is expected be observed. It is also expected that there will be evidence for the rare channel $H \to Z\gamma$ decay, also not yet observed with Run2 data. More details can be found in [8]
A crucial part of the physics program at HL-LHC is the observation of the non-resonant Higgs-boson-pair production, not yet observed so far. The measurement of the Higgs self-coupling, which can be extracted using events of the non-resonant Higgs-boson-pair production is the last missing parameter, not yet measured, in the SM and it's related to the electroweak symmetry breaking mechanics.
The ATLAS collaboration has performed a projection of this measurement assuming 3000 fb^{-1} of pp collisions at a centre-of-mass energy of 14 TeV. using $bbbb$, $bb\gamma\gamma$ and $bb\tau\tau$ final states [9]. The individual significance for the final states are shown in Fig 6, left.
Combining these three final states, the expected signal significance is found to be 3.0(3.5)σ, while the signal strength relative to the Standard Model prediction is expected to be measured with an accuracy of 40(31)%, with(without) systematic uncertainties. The Higgs boson self-coupling can be constrained to $0.4 \leq \lambda_{HHH}/\lambda_{SM} \leq 7.3$, at 95% confidence level, and the measured value of $\lambda_{HHH}/\lambda^{SM}_{HHH}$ is expected to be $1.0^{+0.9}_{-0.8}$.

Publications, internal documents and public presentations:

- ATLAS Collaboration, "HProspects Higgs couplings for YR", ATL-PHYS-PUB-2018-054 (contact editor)

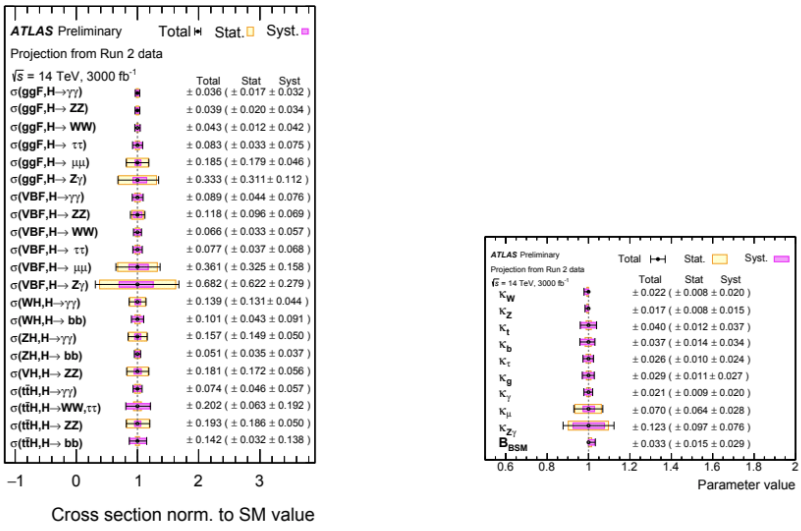

Figure 15: Left: Expected results for the measured cross sections times branching fraction for the ggF, VBF, WH, ZH and $t\bar{t}H$ production modes in each relevant decay channel, normalized to their SM predictions. Right: Expected result for the measurement of each Higgs boson coupling modifier per particle type with effective photon, gluon and $Z\gamma$ couplings, including BSM contribution to the Higgs boson total width. All parameters except t are assumed to be positive. The conditions $\kappa_{W,Z} \leq 1$ are applied. The SM corresponds to $\mathrm{B_{BSM}}$=0 and all κ parameters equal to unity

Channel	Statistical-only	Statistical + Systematic
$HH \to bbbb$	1.4	0.61
$HH \to bb\tau^+\tau^-$	2.5	2.1
$HH \to bb\gamma\gamma$	2.1	2.0
Combined	3.5	3.0

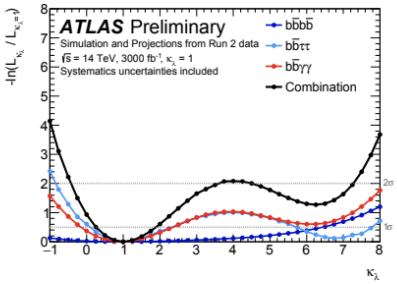

Figure 16: Left: Significance of the individual $HH \to bbbb$, $HH \to bb\tau\tau$ and $HH \to bb\gamma\gamma$ channels as well as their combination. Right: Negative logarithm of the ratio of the maximum likelihood for κ_λ, defined as $\lambda_{HHH}/\lambda_{SM}$, to the maximum likelihood for $\kappa_\lambda = 1$. The black circles show the results for the combination, while the colored markers show the values coming from the individual channels. Systematic uncertainties are included. The dashed lines at 0.5 and 2.0 indicate the values corresponding to the 1σ and 2σ confidence intervals, respectively

- ATLAS Collaboration, "HProspects theory uncertainty impact", ATL-PHYS-PUB-2018-010 (contact editor)
- M.Cepeda et al, "Higgs Physics at the HL-LHC and HE-LHC", arXiv:1902.00134
- M.Testa, Presentation at ICHEP 2018, July 4-11, 2018 Coex, Seoul, "Search for New Physics through the Reconstruction of Challenging Signatures with the ATLAS detector"
- M. Testa, Invited talk "HL-LHC Higgs Physics" at Workshop on the Circular Electron-Positron Collider, EU Edition 2019, 15-17 April 2019

Responsibilities in ATLAS

- Convener of the Higgs Prospects analysis group (April 2017 - October 2019)
- Responsible of Data Quality of offline E_T^{miss} (April 2015 - current)

7 Inner Tracker (ITk) for Phase-II upgrade

After the "Phase-I" upgrade in 2018, the LHC will undergo a "Phase-II" upgrade in 2023, to deliver the instantaneous luminosity of $\sim 7.5 \times 10^{34} cm^{-2} s^{-1}$, more than a factor 10 beyond its design value, corresponding to unprecedented pile-up conditions with an a average of 200

interactions per crossing. The ATLAS detector will be upgraded to maintain its capabilities. In particular the Inner Detector, with acceptance up to $|\eta| < 2.5$, will be substituted by a new, all-silicon Inner Tracker (ITk), whose acceptance will be $|\eta| < 4.0$. The ITk detector comprises two subsystems: a Strip Detector surrounding a Pixel Detector. The ITk layout is shown in Fig.17, left. The Strip Detector (blue), covering $|\eta|$ <2.7, is complemented by a 5 layer Pixel Detector (red) extending the coverage to $|\eta| < 4$. LNF is involved in the construction of one outer pixel endcap of the ITk and in simulation of the performance of the reconstruction of jets and the missing transverse energy.

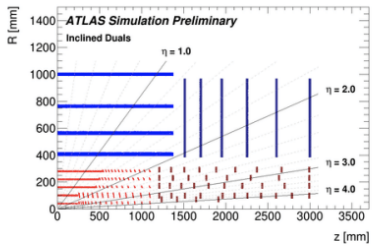

Figure 17: Schematic layout of the ITk. The barrel and endcap for the pixel and strip sub-systems are shown in red and blue respectively. The rings of the pixel endcap are shown as red vertical lines.

7.1 ITk outer-endcap construction

LNF is involved in the construction of one outer endcap of the ITk Pixel detector, being one the integration site. The pixel end-cap system is designed to supply a minimum of at least 9 hits from the end of the strip coverage in pseudorapidity to $|\eta| = 4$. The novel concept is the end-cap ring system, where layers of pixel rings extend the coverage in z and allow routing of the service separately along each ring layer. Each ring can be individually placed to optimise the coverage. More information are in [10]. A 3d model of one outer endcap is shown in Fig.18, left. Each layer of rings is supported by a 0.4mm carbon fiber cylinder shell, along which services for the rings are routed. Each ring is constructed from two half-rings, each covering just over half of the ϕ coverage of the entire ring (Fig.18, right). The two half rings in a pair are separated in z by 10 mm, to allow them to overlap in ϕ such that each ring is hermetic for $p_{\mathrm{T}} = 1$ GeV primary particles. The pixel services (cables, cooling pipes, data lines) are routed from their sources out to Pixel Patch-Panel 1 (PP1). LNF is involved in the design, prototyping and construction of the PP1, and in the endcap prototype design and construction. The design of the prototype of the endcap and the PP1 is shown in Fig.19. The design of the tools for the insertion of the half-rings in the half-shells has started this year.

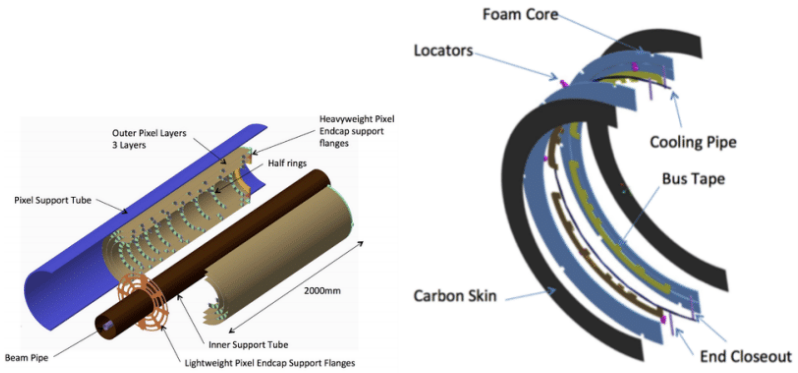

Figure 18: Left: Exploded 3D drawing of one Outer End-cap. Right: Exploded view of the surface of a half-ring

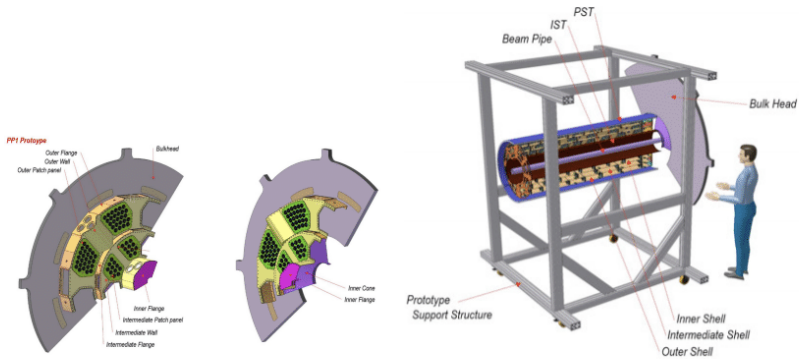

Figure 19: Left: design of the PP1 prototype. Right: design of the endcap prototype.

Publications, internal documents and public presentations:

- S. Tomassini, "Leak Rate Specification for the Pixels PP1", AT2-IP-ES-0008, in progress

Responsabilities in ATLAS

- Local responsible for one pixel endcap integration
- Responsibility of the design and construction of two "patch panels 1"

7.2 Jet/E_{T}^{miss} offline reconstruction performance

There is tremendous potential for improved performance for jets and $\not{E}_T$ in the very forward region. Tracking information can be used by tagging pile-up jets in the forward region as has been done in the central region for Run I and Run II. Forward pile-up jets rejection induces an improvement in $\not{E}_T$ as well. The variable used to study the forward pile-up jet tagging is $R_{pT} = \frac{\Sigma_k p_T^{trk_k}(PV_0)}{p_T^{jet}}$ which computes the scalar sum of the p_T of the charged tracks associated with a particular jet, which are also associated with the primary vertex (PV0), and normalizes this to the p_T of the relevant jet. The rejection of pile-up jets versus the efficiency of the R_{pT} cut for hard-scatter jets is shown in Figure 20, left. The $\not{E}_T$ resolution as a function of the local pile-up density is shown in Figure 20, right. More information are in [10].

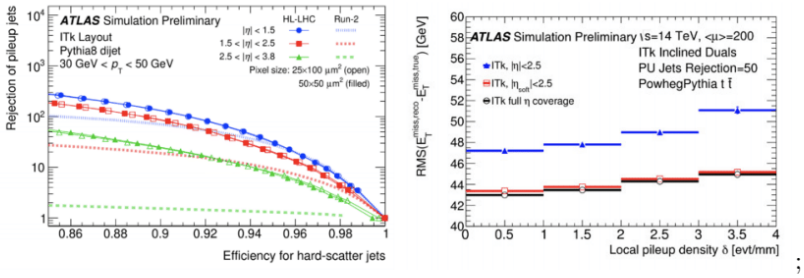

;

Figure 20: Left: The rejection of pile-up jets as a function of the efficiency for hard-scatter jets with $30 < pT < 50$ GeV p_T using the R_{pT} discriminant in di-jet events with an average of 200 pile-up events. Right: The resolution of $\not{E}_T$ in Monte Carlo $t\bar{t}$ events with an average of 200 pile-up events as a function of the local pile-up vertex density around the hard-scattering vertex, for three different $\not{E}_T$ definitions. The first (blue) considers only tracks in the region $|\eta| < 2.5$ for both pile-up jet rejection and soft-tracks not belonging to jets. The second uses tracks for pile-up jet rejection up to $|\eta|$ of 4 (red). The third uses tracks for pile-up jet rejection and soft-tracks up to $|\eta|$ of 4 (black).

Publications, internal documents and public presentations:

- ATLAS Collaboration,"Tracking Performance of the ITk", ATL-PHYS-PUB-2019-014
- ATLAS Collaboration, "Expected performance at HL-LHC", ATL-PHYS-PUB-2019-005
- ATLAS Collaboration,"MissingEt in data 15 + 16 ATLAS", ATL-CONF-PUB-2018-023

References

[1] ATLAS Collaboration, *ATLAS New Small Wheel: Technical Design Report*, Technical Design Report ATLAS. CERN-LHCC-2013-006. CERN, Geneva, 2013

[2] Y. Giomataris et al., *MICROMEGAS: a high-granularity position-sensitive gaseous detector for high particle-flux environments*, Nucl. Instrum. Meth. A 376 29, 1996

[3] M. Iodice [ATLAS Muon Collaboration], *Micromegas detectors for the Muon Spectrometer upgrade of the ATLAS experiment*, JINST 10 (2015) no.02, C02026;

[4] Measurements of the Higgs boson production, fiducial and differential cross sections in the 4l decay channel at $\sqrt{s} = 13$ TeV with the ATLAS detector, ATLAS-CONF-2018-018

[5] F. Maltoni, K. Mawatari and M. Zaro, Higgs characterisation via vector-boson fusion and associated production: NLO and parton-shower effects, Eur. Phys. J. C74 (2014) 2710, arXiv: 1311.1829 [hep-ph].

[6] Handbook of LHC Higgs Cross Sections: 4. Deciphering the Nature of the Higgs Sector (arXiv:1610.07922).

[7] M.Cepeda et al, "Higgs Physics at the HL-LHC and HE-LHC", arXiv:1902.00134

[8] ATLAS Collaboration, "Projections for measurements of Higgs boson cross sections, branching ratios, coupling parameters and mass with the ATLAS detector at the HL-LHC", ATL-PHYS-PUB-2018-054

[9] ATLAS Collaboration, "Measurement prospects of the pair production and self-coupling of the Higgs boson with the ATLAS experiment at the HL-LHC", ATL-PHYS-PUB-2018-053

[10] ATLAS Collaboration, "Technical Design Report for the ATLAS ITk Pixel Detector", ATL-COM-ITK-2017-073